Astronomy & Astrophysics

The OTELO survey

II. The faint-end of the Hα luminosity function at *z* ∼ 0.40

Marina Ramón-Pérez[1,2], Ángel Bongiovanni[1,2,3], Ana María Pérez García[4,3], Jordi Cepa[1,2,3], Maritza A. Lara-López[6], José A. de Diego[7], Emilio Alfaro[8], Héctor O. Castañeda[9], Miguel Cerviño[1,8,4], Mirian Fernández-Lorenzo[8], Jesús Gallego[10], J. Jesús González[7], J. Ignacio González-Serrano[11,3], Jakub Nadolny[1,2], Iván Oteo Gómez[12,13], Ricardo Pérez Martínez[5,3], Irene Pintos-Castro[14], Mirjana Pović[8,15], and Miguel Sánchez-Portal[16,17,3]

[1] Instituto de Astrofísica de Canarias (IAC), 38200 La Laguna, Tenerife, Spain
e-mail: bongio@iac.es
[2] Departamento de Astrofísica, Universidad de La Laguna (ULL), 38205 La Laguna, Tenerife, Spain
[3] Asociación Astrofísica para la Promoción de la Investigación, Instrumentación y su Desarrollo, ASPID, 38205 La Laguna, Tenerife, Spain
[4] Centro de Astrobiología (CSIC/INTA), 28850 Torrejón de Ardoz, Madrid, Spain
[5] ISDEFE for European Space Astronomy Centre (ESAC)/ESA, PO Box 78, Villanueva de la Cañada 28690, Madrid, Spain
[6] Dark Cosmology Centre, Niels Bohr Institute, University of Copenhagen, Juliane Maries Vej 30, 2100 Copenhagen Ø, Denmark
[7] Instituto de Astronomía, Universidad Nacional Autónoma de México, México D.F., Mexico
[8] Instituto de Astrofísica de Andalucía, CSIC, 18080 Granada, Spain
[9] Departamento de Física, Escuela Superior de Física y Matemáticas, Instituto Politécnico Nacional, México D.F., Mexico
[10] Departamento de Astrofísica, Facultad de CC. Físicas, Universidad Complutense de Madrid, 28040 Madrid, Spain
[11] Instituto de Física de Cantabria (CSIC-Universidad de Cantabria), 39005 Santander, Spain
[12] Institute for Astronomy, University of Edinburgh, Royal Observatory, Blackford Hill, Edinburgh EH9 3HJ, UK
[13] European Southern Observatory, Karl-Schwarzschild-Str. 2, 85748 Garching, Germany
[14] Department of Astronomy & Astrophysics, University of Toronto, Canada
[15] Ethiopian Space Science and Technology Institute (ESSTI), Entoto Observatory and Research Center (EORC), Astronomy and Astrophysics Research Division, PO Box 33679, Addis Abbaba, Ethiopia
[16] European Southern Observatory, Alonso de Córdova 3107, Vitacura Casilla 19001, Santiago, Chile
[17] Joint ALMA Observatory, Alonso de Córdova 3107, Vitacura Casilla 763 0355, Santiago, Chile

ABSTRACT

Aims. We take advantage of the capability of the OTELO survey to obtain the Hα luminosity function (LF) at z ∼ 0.40. Because of the deepest coverage of OTELO, we are able to determine the faint end of the LF, and thus better constrain the star formation rate and the number of galaxies at low luminosities. The AGN contribution to this LF is estimated as well.
Methods. We make use of the multiwavelength catalogue of objects in the field compiled by the OTELO survey, which is unique in terms of minimum flux and equivalent width. We also take advantage of the pseudo-spectra built for each source, which allow the identification of emission lines and the discrimination of different types of objects.
Results. The Hα luminosity function at $z \sim 0.40$ is obtained, which extends the current faint end by almost 1 dex, reaching minimal luminosities of $\log_{10} L_{\mathrm{lim}} = 38.5$ erg s^{-1} (or ~0.002 $M_\odot$ yr^{-1}). The AGN contribution to the total Hα luminosity is estimated. We find that no AGN should be expected below a luminosity of $\log_{10} L = 38.6$ erg s^{-1}. From the sample of non-AGN (presumably, pure SFG) at $z \sim 0.40$ we estimated a star formation rate density of $\rho_{\mathrm{SFR}} = 0.012 \pm 0.005\ M_\odot$ yr^{-1} Mpc^{-3}.

Key words. surveys – galaxies: star formation – galaxies: active – galaxies: luminosity function, mass function

1. Introduction

The luminosity function (LF) is an essential empirical tool to evaluate the distribution and large-scale structures of galaxies in the Universe. This function gives the number density Φ (erg s^{-1} Mpc^{-3}) of galaxies per luminosity interval. By tracing specific emission lines across different redshifts, the evolution of star-forming galaxies can also be studied. Given its importance, the LF is usually one of the first things to be derived in any survey. However, this is not always a simple task, as corrections from incompleteness and extinction, among other, must be made (see Johnston 2011 for a review on the topic).

In the case of the Hα emission line, the LF allows us to estimate the star formation rate (SFR) function over different cosmological times (see Gallego et al. 1995), giving invaluable information about the way our Universe has evolved. Sobral et al. (2013) studied the evolution of the Hα LF between redshifts $z = 0.40$ and 2.23, emphasising the high sensitivity of

this SFR tracer by far when compared to widely used proxies in the ultraviolet (UV) or the far-infrared (FIR) domain. Even so, they claim that the evolution seen in Hα LF in the last 11 Gyr is in agreement with those obtained using UV and FIR tracers. A similar agreement (within errors) among these SFR functions have been previously reported by for example Martin et al. (2005) and Bothwell et al. (2011) in the case of local Universe, who sampled some decades in luminosity up to lower limits of $\log_{10} L(\text{UV}; \text{FIR}) = 6\text{--}7 L_\odot$. A similar trend is reported by Magnelli et al. (2009) from measuring the SFR history at $0.4 < z < 1.4$ ($11 < \log_{10} L_{\text{IR}} < 13 L_\odot$), and by Smit et al. (2012) at $z > 4$. However, we identified a significant discrepancy between the results given by Sobral et al. (2013) at low redshift and those of Drake et al. (2013) or Ly et al. (2007), especially at low luminosities, which corresponds to the faint end of the SFR function. Indeed, there is evidence of the strong dependence of the faint-end slope on the environment at selected redshifts, even within the framework of large extragalactic surveys (e.g. Sobral et al. 2011; Geach et al. 2012).

The faint end of the SFR distribution functions allows us to quantify the contribution of low-mass galaxies with mild star formation, which are always more numerous than starburst (i.e. SFR $> 10 M_\odot \text{ yr}^{-1}$) galaxies, to the SFR density estimation at a given epoch. It also provides clues about the processes involved in galaxy formation processes at small dark matter (DM) halo scales and the feedback effects on the star formation of low-luminosity galaxies (Bothwell et al. 2011), in contrast with model predictions (i.e. the dubbed "missing satellite" problem, Klypin et al. 1999; Moore et al. 1999). As a consequence, obtaining deep spectroscopic data to extend the statistics of star-forming galaxies towards very faint luminosities provides vital insights to constrain the SFR functions and unravel the causes behind the inconsistencies cited above.

Complementary to this, there is growing evidence of the role of active galactic nuclei (AGN) in the regulation of star formation processes in their hosts (Azadi et al. 2015). In this sense, the AGN contamination must be taken into account in order to construct the SFR function. Even though the AGN contribution seems to be increased with the stellar mass (e.g. Xue et al. 2010) for a given redshift, the fraction of these objects is unevenly estimated depending on the characteristics of the survey. For instance, Garn et al. (2010) claimed that the overall AGN contamination in their sample is between 5 and 11%, but that these numbers probably underestimate the real rate. Conversely, Sobral et al. (2016) found that 30% of their objects are AGN and that this fraction increases strongly with Hα luminosity; Matthee et al. (2017) also reached the same conclusion. If the AGN population at $z \sim 0.40$ can be figured out, the contribution of active galaxies to the LF can be directly derived without the need of additional assumptions or estimations, as in most works.

In this work, we make use of data from OTELO, an ambitious narrow-band survey using the red tunable filter of the 10.4 m Gran Telescopio Canarias (La Palma, Spain). The OTELO survey targets a 7.5×7.4 arcmin^2 region of the Extended Groth Strip (EGS) with the aim of detecting emission-line sources. To this purpose, a tomography of 36 scans with a full width at half maximum (FWHM) of 12 Å and a sampling interval of 6 Å is made in the range 9070–9280 Å, allowing the construction of a pseudo-spectra for each source in the field. Details on the OTELO survey, the use of tunable filters and its data products are provided in Bongiovanni et al. (2019).

With these characteristics, OTELO has become the deepest emission-line survey to date, unique in terms of minimum flux and equivalent width (EW). In particular, the Hα+[NII] lines are observed in OTELO at $z \sim 0.40$. A multiwavelength catalogue of all the sources detected in the field, with data ranging from X-rays to FIR, has already been compiled. The OTELO multiwavelength catalogue, together with the pseudo-spectra, allow for the identification of the Hα emitters in the field at $z \sim 0.40$ (both AGN and non-AGN), enabling the construction of the corresponding segregated LF.

We therefore aim to take advantage of the capability of OTELO to obtain the Hα LF to extend its faint end and thus constraining the SFR and the number of galaxies at low luminosities. Exploiting the AGN selection and analysis in OTELO survey made by Ramón-Pérez et al. (2019), hereafter referred to as OTELO-III, and carrying out the pertaining diagnostics, the AGN contribution to this LF is also estimated.

This paper is organised as follows. In Sect. 2, the selection and identification of the sample of Hα emitters in OTELO is explained, as well as the Hα line flux measurements and the detection limits in OTELO for this particular line. The construction of the LF is then described in Sect. 3. Finally, Sect. 4 summarises the main conclusions of this work.

Through this paper a standard cosmology with $\Omega_\Lambda = 0.7$, $\Omega_{\text{m}} = 0.3$, and $H_0 = 70 \text{ km s}^{-1} \text{ Mpc}^{-1}$ is assumed for consistency with recent contributions related to the main topic.

2. Identification of Hα emitters, line flux measurements, and detection limits

Emission-line objects in OTELO were first selected using both an automatic algorithm and a visual classification, based on the appearance of emission significant features in the pseudo-spectra from OTELO. Then, their photometric redshifts were obtained using *LePhare* code (Arnouts et al. 1999, Ilbert et al. 2006) and ancillary data from OTELO. A complementary search for emitting candidates was performed by looking for narrow-band excess and the location of OTELO sources in a colour-colour diagram. A detailed description of the first selection of line emitters in OTELO survey is described in Bongiovanni et al. (2019). We focus on the selection of Hα line emitters and the associated detections biases.

2.1. Selection of Hα emitters candidates

Following the methodology described in Bongiovanni et al. (2019), a sample of potential Hα emitters candidates in OTELO was first obtained. It was composed of all the objects selected by one or more of the different methods as follows: by their spectroscopic or photometric redshifts (4 and 108 objects, respectively), location in the colour-colour diagram (32 objects), or narrow-band excess (27 objects).

This selection was deliberately broad enough to ensure a sample as complete as possible of the existing Hα emitters in the OTELO catalogue. A redshift range of $0.30 \leq z \leq 0.50$ was chosen for the search of potential Hα candidates to take into account the dispersion of the photometric redshift estimations, whose accuracy is better than $|\Delta z|/(1 + z) \leq 0.2$ (Bongiovanni et al. 2019). Additionally, 31 emitters that did not fulfil any of the previously mentioned conditions, but whose pseudo-spectra show signs of a possible Hα+[NII] emission, were also included in the sample. In total, the final sample of candidates comprised 202 objects, some of which were selected by more than one of the mentioned criteria. Table 1 lists a summary of the number of Hα emitters candidates selected by each criterion.

Table 1. Selection of Hα candidates sample.

Criterion	N
With $0.37 \leq z_{\mathrm{spec}} \leq 0.42$	4
With $0.30 \leq z_{\mathrm{phot}} \leq 0.50$	108
Selected by colour	32
Selected by narrow-band excess	27
Selected by appearance	31
TOTAL	202

Notes. Column 1: criterion used for the selection of the candidate. Column 2: number of candidates selected with that criterion. Some objects may have been selected by more than one criterion but they are only included in one category, following the order of the list from top to bottom.

2.2. Identification of Hα emitters

To ensure reliable data, each object in the sample of Hα candidates was examined by four independent collaborators. These collaborators used a web-based graphical user interface (GUI) specifically designed as an on-line platform to have an up-to-date dossier of any OTELO source, and as a facility for the analysis of selected objects, in particular the labelling of significant emission/absorption features in the pseudo-spectrum. For this task the GUI includes a line identifier tool that contains an extensive list (available in OTELO survey URL[1]) of relevant traits that would be seen in the pseudo-spectrum at a selected redshift (including the relative strengths depending on the emission-line object type). The GUI includes three main sections: 1) General Analysis, which contains the source identification and the information about the properties of the emission line(s) in its pseudo-spectrum, 2) Image Analysis, where the postage-stamp images of the source in the ancillary photometric bands are analysed to search for possible blended/multiple sources or dropouts and obtain clues about their morphology, and 3) Photo-z Analysis, where the information about spectral energy distribution fitting performed with *LePhare* code, including uncertainties, and the secondary redshift solutions if available, are taken into account to provide a redshift guess that is refined when the line flux is measured. The web-based GUI was designed to accept prepared lists of sources and store value-added data provided by the collaborators after the source analysis, as demonstrated below, but it also can be used as a free browser for visual inspection of individually selected objects.

Considering all the information gathered in the GUI, each one of the 202 Hα candidates was analysed and assigned up to three possible values of redshift by each collaborator, with a corresponding likelihood value or degree of confidence. This likelihood is scaled from $L = 5$ (highly reliable redshift) to $L = 1$ (possible but not very reliable). The probabilities of the redshift of an object to belong (or not) to the OTELO Hα window ($0.37 \leq z \leq 0.42$) were then calculated by comparing and weighting the different values of redshift and the corresponding likelihoods assigned to the object. At the end of the process, an object was considered as a reliable Hα emitter when the first probability exceeded the second emitter. Following this methodology, 46 out of the 202 candidates were finally selected as true Hα emitters.

---

[1] http://www.iac.es/proyecto/otelo

2.3. Hα line flux measurements

The Hα and [NII]6584 fluxes were derived from the individual pseudo-spectra of each Hα emitter previously selected. Flux measurements were carried out by following the methodology in Sánchez-Portal et al. (2015), which assumes infinitely thin lines and has the advantage of yielding non-contaminated fluxes for each line. Hence, a correction for the [NII] contribution in the case of the Hα line flux is not necessary. Moreover, the availability of the fluxes of both lines allow us to diagnostic the AGN-host/star-forming separation, as described in Sect. 3.

2.4. Detection limits in OTELO

The detection limits and other biases of OTELO as a function of the emission-line parameters were obtained from extensive simulations of synthetic pseudo-spectra described below, based on the work in Ramón-Pérez (2017). In our case, the number of false detections was kept under control by doing successive analysis of the emitting objects by independent collaborators (see Sect. 2.2). However, the number of missing objects had to be estimated. Therefore, the aim of the simulation we performed in this work was to find the detection limits of OTELO survey in terms of EW, so as to see what kind of objects were escaping our detection when searching for Hα emitters. To do so, we simulated an Hα emission line in the form of a Gaussian and then convolved it to the spectral signature of OTELO to obtain its pseudo-spectrum. Three independent variables of the Hα Gaussian were varied: its FWHM, its continuum flux density, and its amplitude. After ranging the grid of these variables a total of 500 independent simulations were performed. Each simulation is composed by one synthetic pseudo-spectrum for each node of the simulation grid in the FWHM-continuum-amplitude space. The synthetic pseudo-spectra are affected by random sky plus photon noise components scaled to the noise distribution of each resulting slice images of the OTELO tomography. Each spectrum was then convolved by the instrumental response of the tunable filter scan to obtain the simulated pseudo-spectra. We then checked whether the resulting pseudo-spectra were detected as emitters using the automatic algorithm for line detection mentioned above.

As an example, Fig. 1 shows the mean value of detection of the pseudo-spectra, given the original FWHM and amplitude of the Hα emission line. There, a value of 0 means that the resulting pseudo-spectrum was never detected as an emitter, while a value of 1 means it was detected in the 500 runs of the simulation. We can see that for higher values of the amplitude and lower values of the FWHM, the detection fraction increases.

In order to draw physical conclusions from the simulation, we computed for each experiment (i.e, for each combination of FWHM, continuum, and amplitude values) the EW of the Hα line. We determined the minimum detected EW for a given probability threshold p (i.e. considering a level of detection of at least $p \times 100\%$ in the whole simulation). For a probability threshold of $p \geq 0.50$, for instance, the minimum detected EW is ~5 Å, while it is ~10.5 Å for a threshold of $p \geq 0.95$. In Fig. 2 we plot the percentage of detected objects in the simulation for those values of probability threshold as a function of the EW. Typical values of Hα EWs for various astrophysical objects, taken from the works of Gavazzi et al. (2006), Gallego et al. (1997), Stern & Laor (2012), and Gil de Paz et al. (2003), are also indicated.

To summarise, the main results that can be drawn from the simulation about the detection limits of the Hα line in OTELO survey are the following.
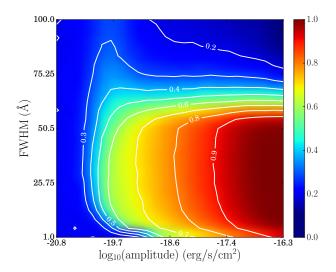
Fig. 1. Mean value of detection in the 500 runs of the simulation (0: never detected as emitter, 1: always detected as emitter), given the FWHM and the amplitude of the Hα Gaussian. The continuum variable has been collapsed in the plane of the other two. White lines represent the detection probability contours.

With a probability threshold of 50% ($p \geq 0.50$) we should be able to detect
- about 1 out of 5 elliptical galaxies with EW = 6 Å.
- more than 75% of spiral galaxies with EW $\geq$ 60 Å.
- between 62% and 79% of the galaxies with $100 \leq$ EW ≤ 200 Å.
- between 55% and 60% of the galaxies with EW ≥ 200 Å.

We reach a minimum EW of
- 5 Å with a probability of $p \geq 0.50$ for objects with a minimum flux density in the pseudo-continuum of $\sim 10^{-19}$ erg s^{-1} cm^{-2} Å^{-1}.
- 10.5 Å with a probability of $p \geq 0.95$ for objects with a minimum flux density in the pseudo-continuum of $\sim 10^{-18}$ erg s^{-1} cm^{-2} Å^{-1}.

The results of this simulation are crucial in order to estimate the incompleteness of the sample of objects when deriving the Hα LF (see Sect. 3).

3. Luminosity function at $z \sim 0.40$

In this work, we obtained the Hα LF at $z \sim 0.40$ and used this set of values to study the AGN contribution to the total luminosity at that redshift. The main advantage of OTELO, when compared to other surveys, is that emitters and AGN at $z \sim 0.40$ have been carefully inspected and selected. From the sample of Hα emitters composed by 46 OTELO sources selected at $z \sim 0.40$, a total of 12 were optically classified as narrow- or broad-line AGN. The latter sources were segregated from the sample by using the EWαn2 diagnostic (Cid Fernandes et al. 2010), in which the [OIII]/Hβ ratio of the usual BPT diagram (Baldwin et al. 1981) is replaced by the EW of Hα at rest-frame. We adopted the prescription given by Stasińska et al. (2006) to separate pure star-forming galaxies from composite/AGN hosts in the sample. More details about this particular topic and the AGN demographics in OTELO are given in OTELO-III. This implies that the AGN contribution in each luminosity interval is exactly known and not only estimated, as in other works (see e.g. Shioya et al. 2008 or Sobral et al. 2013).
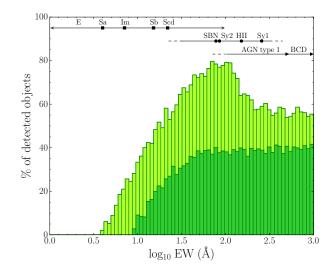
Fig. 2. Percentage of detected objects in the simulation depending on the EW of the input Hα Gaussian line. Light green: $p \geq 0.50$ probability threshold. Dark green: $p \geq 0.95$ probability threshold. Typical values of Hα EWs for multiple astrophysical objects are also indicated. Black squares: median values of EW as in Gavazzi et al. (2006). Black circles: mean values as in Gallego et al. (1997). Black triangles: maximum values from Stern & Laor (2012) and Gil de Paz et al. (2003).

3.1. Completeness correction

One of the main difficulties when deriving the LF is to estimate (and correct) the incompleteness of the sample of objects. In this work, we take advantage of the simulations described in Sect. 2.4, which evaluated the detection probability of an Hα emission line at $z \sim 0.40$ in OTELO. We calculated the mean detection probability as a function of the line flux, for the simulated objects having $p \geq 0.50$, which is the completeness cut that we adopted. The result is shown in Fig. 3. We then fitted the data to a sigmoid function such as $d = aF_1/\sqrt{c - F_1^2}$, where $F_1 = \log(f_1) - b$, f_1 is the line flux. The values obtained from a least-squares fitting using the Levenberg-Marquardt algorithm implemented in IDL were $a = 0.916 \pm 0.005$, $b = 19.187 \pm 0.047$, and $c = 0.072 \pm 0.023$. This function was used as our LF completeness correction.

3.2. Volume sampled and cosmic variance

According to the specific characteristics of the OTELO TF-tomography in the spectral dimension and the effective field of view (FoV) sampled, we estimated the comoving volume limited by the Hα line at $0.37 \leq z_{\rm spec} \leq 0.42$, amounting 1.4×10^3 Mpc^3. Because of the relatively small volume of Universe probed for this emission line, the effects of the cosmic variance are not negligible; see Stroe & Sobral 2015 to better understand the impact of this effect on the LF determination. The mean comoving number density of all the OTELO Hα sources is 0.033 Mpc^{-3}. Following Somerville et al. (2004) we estimated a galaxy bias b of ~ 0.77 for this number density, and a variance of DM, $\sigma_{\rm DM} = 0.95$ for such a volume. Accordingly, a general cosmic variance is $\sigma_{\rm v} = b\,\sigma_{\rm DM} \simeq 0.73$ in this science case.

3.3. Hα luminosity function

The LF calculation starts by computing the number Φ of galaxies per unit volume and per unit of Hα luminosity, in bins of
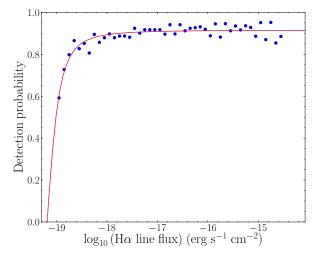
Fig. 3. Mean detection probability as a function of Hα line flux (blue dots) for simulated objects having $p \geq 0.50$ (see Sect. 2.4). The red line indicates the best least-squares fitting of a sigmoid function (see description in the text).

Table 2. Hα LFs (corrected by dust extinction and completeness) at $z \sim 0.40$ for the OTELO survey, considering all the objects in the sample (46) and the non-AGN only (34).

Hα sample	$\log_{10} L(\mathrm{H}\alpha)$ (erg s^{-1})	$\log_{10} \phi$ (Mpc^{-3}dex^{-1})
OTELO [all galaxies]	38.70	$-1.697^{+0.11}_{-0.15}$
	39.20	$-1.782^{+0.12}_{-0.17}$
	39.70	$-1.745^{+0.12}_{-0.16}$
	40.20	$-2.089^{+0.16}_{-0.26}$
	40.70	$-2.488^{+0.23}_{-0.53}$
	41.20	$-2.489^{+0.23}_{-0.53}$
OTELO [non-AGN]	38.70	$-1.776^{+0.12}_{-0.17}$
	39.20	$-1.828^{+0.13}_{-0.18}$
	39.70	$-1.883^{+0.13}_{-0.19}$
	40.20	$-2.186^{+0.18}_{-0.30}$
	40.70	$-2.789^{+0.30}_{-2.40}$
	41.20	$-2.790^{+0.30}_{-2.40}$

Notes. Errors are subject to Poissonian statistics only.

$\Delta[\log L(\mathrm{H}\alpha)] = 0.5$. We used the $V_{\max}$ method (Schmidt 1968; see, for instance, Eq. (2) in Bongiovanni et al. 2005 or Eq. (8) in Hayashi et al. 2018) with the following adapted expression:

$$\Phi[\log_{10} L(\mathrm{H}\alpha)] = \kappa \frac{4\pi}{\Omega} \sum_i \frac{1}{d_i}, \qquad (1)$$

which takes into account the volume of Universe surveyed and the completeness bias in our survey: d_i is the detection probability for the ith galaxy, Ω is the observed solid angle ($\sim 4.7 \times 10^{-6}$ str), and κ is a normalisation factor proportional to $V_{\max}^{-1}$ ($\kappa = V_{\max}^{-1} \times \Delta[\log L(\mathrm{H}\alpha)]^{-1}$); the maximum comoving volume is limited by the Hα line in OTELO spectral range.

The Hα sample was corrected from completeness following the function shown in Fig. 3 and also from dust attenuation, using the reddening value given by the best spectral energy distribution fit from *LePhare* for each galaxy. We used the empirical relation by Ly et al. (2012), which connects the dust reddening $E(B-V)$ and the extinction $A_{\mathrm{H}\alpha}$ for galaxies at $z \sim 0.50$: $A_{\mathrm{H}\alpha} = 1.85 \times E(B-V) \times k(\mathrm{H}\alpha)$, where $k(\mathrm{H}\alpha) = 3.33$ and the proportionality factor comes from the ratio between stellar and nebular reddening as follows: $E(B-V)_{\mathrm{gas}} = 1.85 \times E(B-V)$ (Calzetti et al. 2000).

Using the aforementioned expressions, a completeness and dust extinction-corrected Hα LF at $z \sim 0.40$ was obtained (see Table 2) for the OTELO complete data set (46 objects) and for the OTELO star-forming galaxies sample (34 objects). A Schechter function (Schechter 1976) was then fitted to our data points. Accounting for our low number statistics for the determination of the LFs, and following the data weighting analysis in Comparat et al. (2015), we adopted the ratio of the number of galaxies within each luminosity bin to the total number in each subsample as weighting scheme in our fitting. The Schechter parameters of the OTELO LFs for each subsample are given in Fig. 4, along with those obtained by previous works for Hα emitters at the same redshift. Main error sources in our LFs are those of statistical nature (i.e. obeying a Poissonian process) and those derived from the cosmic variance effects. The contribution of these uncertainties were summed in quadrature and dominate by far over those that come from the line flux calculations and those corresponding to the detection probability function

represented in Fig. 3. For this reason the latter sources of error were dismissed in our LF estimations.

The characteristics of OTELO survey makes it very competitive in terms of depth and recovery of the LF faint end. As can be seen in Fig. 4, OTELO data reach luminosities almost 1 dex fainter than the faintest limit of the deepest survey (Ly et al. 2007). However, owing to its small angular coverage and number statistics, the LF bright end of OTELO is poorly sampled. That is why we decided to fix the L^* parameter and take the mean value $\bar{L}^*$ from the LFs of Drake et al. (2013), Sobral et al. (2013) and Ly et al. (2007): $\log_{10} \bar{L}^*$ (erg s^{-1}) $= 41.85$. The dispersion in $\bar{L}^*$ from data in those works is small ($\sigma_{\bar{L}^*} = 0.16$), reinforcing our assumption. Besides, the strength of OTELO resides in its depth, and hence in determining the slope at the faint end, α. This parameter and ϕ^* were obtained by fitting the Schechter function to our data points. Their values, as well as those obtained by the already mentioned works, are shown in Table 3.

The OTELO LFs allow us to extend the luminosity range almost 1 dex fainter than previous works such as Ly et al. (2007). The LF of Sobral et al. (2013) seems to deviate from the rest at faint luminosities, overestimating the number of low-luminosity objects. However, given the luminosity limits of their survey, this should not be surprising. The work of Sobral et al. (2013) is, nevertheless, a good reference for the bright end of the LF, taking into consideration the relatively large comoving volume by them explored (see Table 3). It is also worth noticing the potential of OTELO survey to recover and extend the LF, in spite of the small number of objects under study in our sample. As a matter of fact, the samples from works by Drake et al. (2013), Sobral et al. (2013), and Ly et al. (2007) have 6.5, 19, and 9 times more galaxies than our own, respectively, and with ~4 to 60 times the comoving volume explored by OTELO at this redshift. Even so, at the faint end, OTELO's Hα LF at $z = 0.4$ is in agreement with the extrapolation of the SFR function of Drake et al. (2013), with a shallower slope compared to those provided by Ly et al. (2007) and Sobral et al. (2013).

The 34 objects in our sample of Hα emitters that were not selected as AGN are presumably star-forming galaxies. By studying their LF, the SFR can be derived following the standard calibration of Kennicutt (1998), which assumes a Salpeter initial mass function (IMF) with masses between 0.1 and 100 $M_\odot$:

$$\mathrm{SFR}(M_\odot \, \mathrm{yr}^{-1}) = 7.9 \times 10^{-42} L(\mathrm{H}\alpha) (\mathrm{erg \, s}^{-1}). \qquad (2)$$
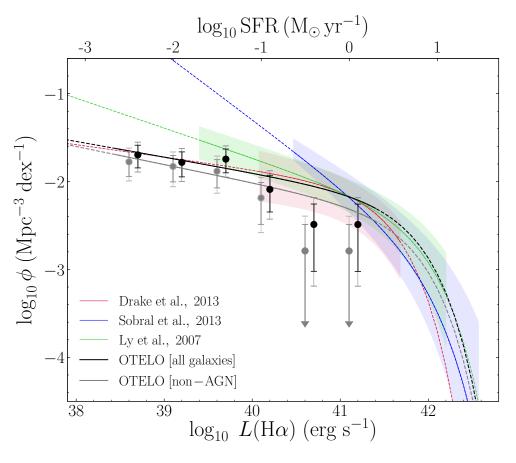
Fig. 4. Completeness and dust extinction-corrected Hα LFs at $z \sim 0.40$. The black line corresponds to the LF fitting for the whole sample of OTELO emitters at that redshift, which are represented with black dots, while the grey line is the LF fitting for the non-AGN population (grey circles). For the sake of clarity, grey circles are displaced -0.1 dex in luminosity with respect to black circles. Shorter error bars are Poissonian and the larger error bars have the cosmic variance uncertainties evenly added in quadrature (see text for details). The Hα LFs of Drake et al. (2013), Sobral et al. (2013), and Ly et al. (2007) are plotted in red, blue, and green, respectively. In each case, the solid line represents their sampled luminosity interval, while the dashed line is the extrapolation of their Schechter function fit. The coloured regions are the maximum envelopes that enclose binned data and their corresponding errors as reported by the cited authors.

Table 3. Schechter parameters of the dust-corrected Hα LFs for the OTELO survey and earlier works, all at $z \sim 0.40$.

Data set	Number of sources (N)	Volume (10^3 Mpc^3)	$\log_{10} L_{\rm lim}$ (erg s^{-1})	$\log_{10} \phi^*$ (Mpc^{-3} dex^{-1})	$\log_{10} L^*$ (erg s^{-1})	α	$\log_{10} \mathcal{L}$ (erg s^{-1} Mpc^{-3})	$\rho_{\rm SFR}$ ($M_\odot$ yr^{-1} Mpc^{-3})
Ly et al. (2007)	391	4.71	39.6	-2.75 ± 0.16	41.93 ± 0.19	-1.34 ± 0.06	39.31 ± 0.08	0.016 ± 0.003
Drake et al. (2013)	271	29.5	40	$-2.44^{+0.14}_{-0.17}$	$41.55^{+0.13}_{-0.11}$	$-1.14^{+0.14}_{-0.13}$	39.15 ± 0.02	0.0113 ± 0.0005
Sobral et al. (2013)	797	88	40.5	$-3.12^{+0.10}_{-0.34}$	$41.95^{+0.47}_{-0.12}$	$-1.75^{+0.12}_{-0.08}$	39.55 ± 0.22	0.03 ± 0.01
OTELO [all galaxies]	42 ($< L*$)	1.4	38.7	-2.59 ± 0.22	41.85 (fixed)	-1.18 ± 0.08	39.31 ± 0.18	–
OTELO [non-AGN]	33 ($< L*$)	"	38.7	-2.75 ± 0.19	41.85 (fixed)	-1.21 ± 0.07	39.17 ± 0.16	0.012 ± 0.005

Integrating this LF we obtain a value of $\log_{10} \mathcal{L}(\mathrm{H}\alpha) = 39.17 \pm 0.16$, which translates into a SFR density of $\rho_{\rm SFR} = 0.012 \pm 0.005 \, M_\odot$ yr^{-1} Mpc^{-3} at $z \sim 0.40$. This value is in agreement with that provided by Drake et al. (2013), but it is also consistent with other obtained by previous works (see last column in Table 3). It is worthy of note that this estimation does not include the contribution of the AGN hosts to the star formation budget in the comoving volume explored. Our SFR density estimation is closer to that of Ly et al. (2007) and Drake et al. (2013), while the value obtained by Sobral et al. (2013) departs from the rest and probably tends to overestimate the SFR for the aforementioned reasons.

3.4. Role of AGN hosts

The AGN contribution to the total Hα luminosity at $z \sim 0.40$ is estimated by comparing the OTELO LF obtained for the complete sample of emitters and that obtained for the sample of star-forming galaxies only, both represented in Fig. 4. The ratio of the LFs given in Table 2 is represented in Fig. 5), and it can be

fitted with a linear function with the following parameters:

$$\log_{10} \left(\frac{\phi_{\text{[all galaxies]}}}{\phi_{\text{[non−AGN]}}} \right) = a \times \log_{10} L(\mathrm{H}\alpha) + b, \quad (3)$$

$a = 0.119 \pm 0.033$

$b = -4.577 \pm 1.335$.

The contribution of AGN hosts in the Hα luminosity range explored by OTELO at $z = 0.4$ tends to increase monotonically up to a factor ~ 1.5 starting from $\log_{10} L(\mathrm{H}\alpha)$ (erg s^{-1}) $\gtrsim 38.6$. Therefore, it would not be expected to find galaxies hosting AGN at $z \sim 0.4$ below that luminosity threshold. This trend is in agreement with the results obtained by Sobral et al. (2016) and Matthee et al. (2017). In this sense, Gunawardhana et al. (2013) found that the highest AGN contribution in the Hα LFs occurs at $0.17 < z < 0.24$, even though this effect is almost negligible at $z < 0.1$.

Given the small number of objects in our Hα sample for the construction of the LFs, the above results about the AGN contribution should be taken with caution. However, it is worth
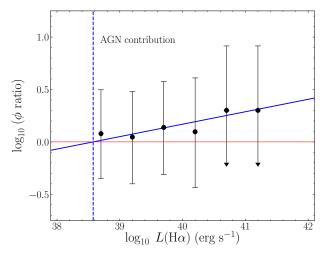
Fig. 5. Ratio between the OTELO Hα LF of the total sample of emitters at $z \sim 0.40$ and that of the star-forming galaxies only. Bars are the sum in quadrature of the Poissonian errors of both LF, as given in Table 2. The blue solid line represents a error-weighted linear fitting to the ratio values. The red horizontal line corresponds to a ratio equals unity. The blue dashed vertical line represents the luminosity above which the AGN contribution becomes relevant.

noticing that the general procedure is addressed to estimate the fraction of AGN as a percentage over the total population, and correct the sample of galaxies accordingly to build the LF. The OTELO survey, in contrast, has allowed us to obtain a complete sample of Hα emitters, for which the AGN fraction is accurately known at each luminosity interval, despite the small comoving volume sampled.

4. Conclusions

This work has focussed on the OTELO survey, an emission-line object survey using the red tunable filters of the OSIRIS instrument at the Gran Telescopio Canarias (Bongiovanni et al. 2019). Following the selection of emitting objects described in Bongiovanni et al. (2019), Hα emitters candidates at $z \sim 0.40$ have been identified and a sample of 46 emitters has been selected.

Then, an Hα LF at $z \sim 0.40$ has been constructed, using a completeness correction derived from a simulation of the detection limits in OTELO and a dust extinction correction from the photo-z estimation (Bongiovanni et al. 2019). Using a mean value of $\log_{10} \bar{L}^*$ (erg s^{-1}) $= 41.85$ ($\sigma_{\bar{L}^*} = 0.16$) calculated from data of previous works, we fitted our data points to a Schechter function with the following parameters for the whole sample of Hα emitters: $\log_{10} \phi^* = -2.59 \pm 0.22$ and $\alpha = -1.18 \pm 0.08$. Using the EWαn2 diagnostic (Cid Fernandes et al. 2010), we removed the AGN from the previous sample and obtained a second LF for non-AGN only with the following parameters: $\log_{10} \phi^* = -2.75 \pm 0.19$ and $\alpha = -1.21 \pm 0.07$.

When compared to previous works, our LFs extend the faint end almost 1 dex, reaching observed Hα luminosities as low as $\log_{10} L_{\mathrm{lim}}$(erg s^{-1}) $= 38.5$ (equivalent to a SFR of $\sim 0.002 \, M_\odot$ yr^{-1}), and therefore constricting the faint-end slope at such luminosity regime.

The AGN contribution to the total Hα luminosity has been estimated. We find that no AGN should be expected below a luminosity of $\log_{10} L_{\mathrm{lim}}$(erg s^{-1}) $= 38.6$. Above this value, the

AGN contribution grows with the luminosity, in agreement with previous works. Again, given our small sample of AGN at $z \sim 0.40$, a study with more statistical significance should be conducted to confirm this result. Discarding AGN hosts contribution to the star formation, we obtained an integrated Hα luminosity from star-forming galaxies at $z = 0.40$ of $\log_{10} \mathcal{L}$ (erg s^{-1}) $= 39.17 \pm 0.16$, yielding a SFR density of $\rho_{\mathrm{SFR}} = 0.012 \pm 0.005 \, M_\odot$ yr^{-1} Mpc^{-3}.

References

Arnouts, S., Cristiani, S., Moscardini, L., et al. 1999, MNRAS, 310, 540
Azadi, M., Aird, J., Coil, A. L., et al. 2015, ApJ, 806, 187
Baldwin, J. A., Phillips, M. M., & Terlevich, R. 1981, PASP, 93, 5
Bongiovanni, A., Bruzual, G., Magris, G., et al. 2005, MNRAS, 359, 930
Bongiovanni, A., Ramón-Pérez, M., Perez Garcia, A., et al. 2019, A&A, 631, A9
Bothwell, M. S., Kennicutt, R. C., Johnson, B. D., et al. 2011, MNRAS, 415, 1815
Calzetti, D., Armus, L., Bohlin, R. C., et al. 2000, ApJ, 533, 682
Cid Fernandes, R., Stasińska, G., Schlickmann, M. S., et al. 2010, MNRAS, 403, 1036
Comparat, J., Richard, J., Kneib, J.-P., et al. 2015, A&A, 575, A40
Drake, A. B., Simpson, C., Collins, C. A., et al. 2013, MNRAS, 433, 796
Gallego, J., Zamorano, J., Aragon-Salamanca, A., & Rego, M. 1995, ApJ, 455, L1
Gallego, J., Zamorano, J., Rego, M., & Vitores, A. G. 1997, ApJ, 475, 502
Garn, T., Sobral, D., Best, P. N., et al. 2010, MNRAS, 402, 2017
Gavazzi, G., Boselli, A., Cortese, L., et al. 2006, A&A, 446, 839
Geach, J. E., Sobral, D., Hickox, R. C., et al. 2012, MNRAS, 426, 679
Gil de Paz, A., Madore, B. F., & Pevunova, O. 2003, ApJS, 147, 29
Gunawardhana, M. L. P., Hopkins, A. M., Bland-Hawthorn, J., et al. 2013, MNRAS, 433, 2764
Hayashi, M., Tanaka, M., Shimakawa, R., et al. 2018, PASJ, 70, S17
Ilbert, O., Arnouts, S., McCracken, H. J., et al. 2006, A&A, 457, 841
Johnston, R. 2011, A&ARv, 19, 41
Kennicutt, Jr., R. C. 1998, ARA&A, 36, 189
Klypin, A., Kravtsov, A. V., Valenzuela, O., & Prada, F. 1999, ApJ, 522, 82
Ly, C., Malkan, M. A., Kashikawa, N., et al. 2007, ApJ, 657, 738
Ly, C., Malkan, M. A., Kashikawa, N., et al. 2012, ApJ, 747, L16
Magnelli, B., Elbaz, D., Chary, R. R., et al. 2009, A&A, 496, 57
Martin, D. C., Seibert, M., Buat, V., et al. 2005, ApJ, 619, L59
Matthee, J., Sobral, D., Best, P., et al. 2017, MNRAS, 471, 629
Moore, B., Ghigna, S., Governato, F., et al. 1999, ApJ, 524, L19
Ramón-Pérez, M. 2017, PhD Thesis, Universidad de La Laguna, Spain
Ramón-Pérez, M., Bongiovanni, Á., Pérez García, A. M., et al. 2019, A&A, 631, A11
Sánchez-Portal, M., Pintos-Castro, I., Pérez-Martínez, R., et al. 2015, A&A, 578, A30
Schechter, P. 1976, ApJ, 203, 297
Schmidt, M. 1968, ApJ, 151, 393
Shioya, Y., Taniguchi, Y., Sasaki, S. S., et al. 2008, ApJS, 175, 128
Smit, R., Bouwens, R. J., Franx, M., et al. 2012, ApJ, 756, 14
Sobral, D., Best, P. N., Smail, I., et al. 2011, MNRAS, 411, 675
Sobral, D., Smail, I., Best, P. N., et al. 2013, MNRAS, 428, 1128
Sobral, D., Kohn, S. A., Best, P. N., et al. 2016, MNRAS, 457, 1739
Stroe, A., & Sobral, D. 2015, MNRAS, 453, 242
Somerville, R. S., Lee, K., Ferguson, H. C., et al. 2004, ApJ, 600, L171
Stasińska, G., Cid Fernandes, R., Mateus, A., Sodré, L., & Asari, N. V. 2006, MNRAS, 371, 972
Stern, J., & Laor, A. 2012, MNRAS, 423, 600
Xue, Y. Q., Brandt, W. N., Luo, B., et al. 2010, ApJ, 720, 368